Available online at www.sciencedirect.com
SCIENCE DIRECT®
ELSEVIER
International Journal of Solids and Structures 42 (2005) 3471–3485
INTERNATIONAL JOURNAL OF SOLIDS and STRUCTURES
www.elsevier.com/locate/ijsolstr

Fourier analysis of X-ray micro-diffraction profiles to characterize laser shock peened metals

Hongqiang Chen [a,*,1], Y. Lawrence Yao [a], Jeffrey W. Kysar [a], I. Cev Noyan [b], Youneng Wang [a]

[a] *Department of Mechanical Engineering, Columbia University, 500 West 120th Street, 220 S.W. Mudd, New York, NY 10027, United States*
[b] *Thin Film Metallurgy Department, IBM T.J. Watson Research Center, Yorktown Heights, NY 10598, United States*

Received 27 April 2004; received in revised form 18 October 2004
Available online 15 December 2004

Abstract

X-ray micro-diffraction profiles using a synchrotron light source were analyzed via Fourier transformation for single crystal Aluminum and Copper samples subjected to micro-scale laser shock peening. Specifically, the asymmetric and broadened diffraction profiles registered across the shock peen region were observed and analyzed by classic Warren and Averbach (W–A) method [Warren, B.E., Averbach, B.L., 1950. The effect of cold-work distortion on X-ray patterns. Journal of Applied Physics 21, 595–599] and modified W–A method [Ungar, T., Borbely, A., 1996. The effect of dislocation contrast on X-ray line broadening: A new approach to line profile analysis. Applied Physics Letters 69, 3173–3175]. Average strain deviation, mosaic size and dislocation density were estimated for the first time with a spatial resolution of 5 μm. The results compare well with the simulation results obtained from FEM analysis and from electron backscatter diffraction (EBSD) measurements. Differences in response caused by different materials and crystalline orientations (1 1 0 and 0 0 1) were also studied.

Keywords: Fourier analysis; X-ray micro-diffraction; Laser shock peening; Electron backscatter diffraction

* Corresponding author. Tel./fax: +1 631 784 6100.
E-mail address: hchen@quantronixlasers.com (H. Chen).
[1] Current contact information: Quantronix, East Setauket, NY.

0020-7683/$ - see front matter © 2004 Elsevier Ltd. All rights reserved.
doi:10.1016/j.ijsolstr.2004.10.026

1. Introduction

Micro-scale laser shock peening (μLSP) is a technique that can potentially be applied to manipulate the residual stress distribution in surface layers of metal structures with micron-level spatial resolution and thus improve the fatigue and reliability performances of micro-devices (Zhang and Yao, 2001). It is desirable to directly measure strain/stress distributions of the shocked area and study the micro-structure change after μLSP. However, the spatial resolution of conventional X-ray diffraction is typically larger than 0.5 mm, which is too large to map out the residual stress/strain distributions (Zhang and Yao, 2000). Recently, by using X-ray micro-diffraction technology, for the first time, micron level spatial resolution (down to 5 μm) of residual stress distribution on the surface of shock peened single crystal Al and Cu was measured with micron spatial resolution (down to 5 μm) for the first time (Chen et al., 2004).

According to Chen et al. (2004), asymmetric and broadened diffraction profiles were observed at each location in the shock peened region, and analyzed by the sub-profiling method and explained in terms of the heterogeneous dislocation cell structure. Residual stress distribution was obtained as a result. To achieve a better understanding of micro-structure evolution during the process, the spatial distribution of inhomogeneous strain, mosaic size and dislocation density caused by μLSP need to be further studied from the measured X-ray micro-diffraction profile.

Broadening of X-ray diffraction line profiles is caused by non-ideal optics of the instrument and structural imperfections of the specimen. The structural line broadening is often subdivided into size broadening and strain broadening. Size broadening is caused by the finite size of "domains diffracting essentially incoherently with respect to one another" (Warren, 1969). Strain broadening is caused by varying displacements of the atoms with respect to their reference-lattice positions. The classical method to evaluate size and strain broadening using Fourier series coefficients of reflection was developed by Warren and Averbach (1950).

Ungar and Borbely (1996) evaluated dislocation density using X-ray profile analysis of broadened diffraction lines in single Cu crystals deformed in single slip in tension, following a number of attempts (Warren and Averbach, 1950; Wilson, 1942; Krivoglaz and Ryaboshapka, 1963).

In this paper, by using classical Warren and Averbach method (Warren and Averbach, 1950) and its modification (Ungar and Borbely, 1996), the spatial distribution of inhomogeneous strain deviation, mosaic size and dislocation density were evaluated through Fourier analysis of X-ray micro-diffraction profiles for single crystal Al and Cu subjected to μLSP. The result was also compared with other simulation and experimental method such as FEM and EBSD. This analysis directly complements measurements of residual strain/stress in Chen et al. (2004).

2. Experimental and simulation condition

Well-annealed single crystals of 99.999% pure Aluminum and Copper (grown by the seeded Bridgman technique) were used for micro-scale laser shock peening. In order to achieve high diffraction intensity and study the difference caused by crystal orientation, low order orientations of (1 1 0) and (0 0 1) are chosen for two Al samples (surface normal) and the orientation of Copper is (1 1 0) as well. The Laue diffraction method was used to determine the crystal orientation within $\pm 1^\circ$ and the sample was cut to size using a wire EDM (electrical discharge machining).

The sample geometry and μLSP setup is shown in Fig. 1. In order to obtain the deformation symmetry, laser shock peening was applied along [1 1 0] direction in all sample to create a shock line. A frequency tripled Q-switched Nd:YAG laser (wavelength 355 nm) in TEM_{00} mode was employed with pulse duration of 50 ns; spacing between consecutive pulses along the shock line was 25 μm. The laser beam diameter was 12 μm and laser intensity was about 4 GW/cm^2. A thin layer of vacuum grease was spread evenly on the polished sample surface and a 16 μm thick Aluminum foil, chosen for its relatively low threshold of

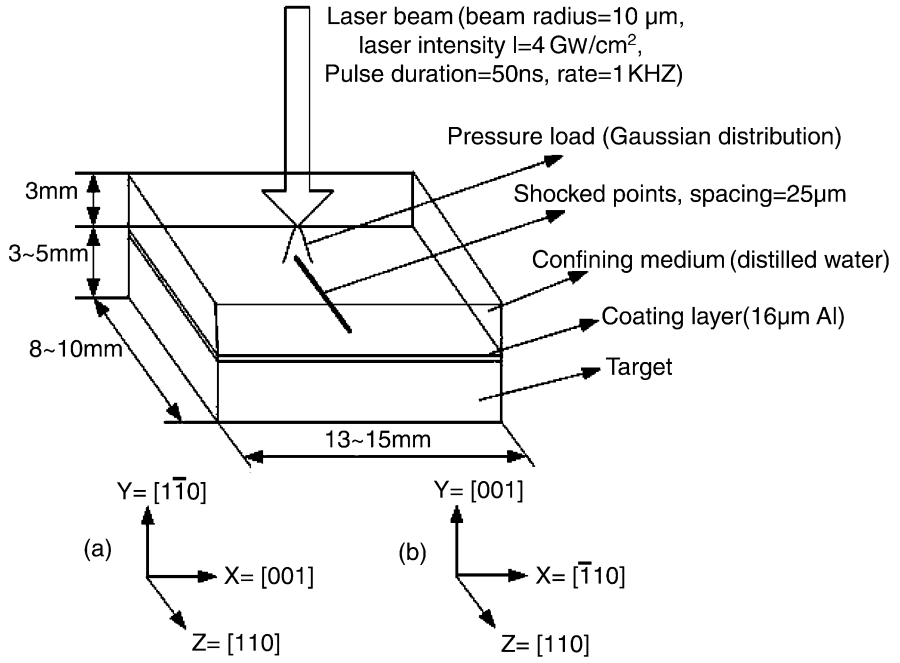

Fig. 1. Sample geometry and laser shock peening condition (dimensions are approximate and may vary slightly among samples). (a) Al(1 1̄ 0) sample and Cu(1 1̄ 0) sample. (b) A1(0 0 1) sample.

vaporization, was tightly pressed onto the grease. The sample was placed in a shallow container filled with distilled water around 3 mm above the sample's top surface. Details of micro-scale LSP setup and sample preparation are referred to Zhang and Yao (2000, 2001), Chen et al. (2004).

In order to understand the overall characteristics of the deformation, the process was also modeled via finite element method (FEM). A commercial FEM code, ABAQUS (Hibbit, Karlsson and Sorensen Inc., 2002), was used for the simulation. Based on the theory of Asaro (1983), a user-material subroutine for single crystal plasticity written by Huang (1991) and modified by Kysar (1997) is incorporated into the finite element analysis. Two orientations, Al(1 1 0) and Al(0 0 1) and two materials Al(1 1 0) and Cu(1 1 0) are simulated with a 2D plane strain assumption. Detail about FEM simulation can be found in Chen et al. (2004).

3. Post-peening material characterization

A high brightness X-ray beam (beamline X20A) of National Synchrotron Light Source at Brookhaven National Lab was used in diffraction and the beam size was around 5–7 μm. Monochromatic synchrotron radiation at 8.0 KeV ($\lambda = 1.54024$ Å) was used. Multiple measurement points were chosen along a line perpendicular to a shocked line. The spacing between adjacent measurement points varies from 10 μm (from ±100 μm away from the center of the shocked line) to 5 μm within ±20 μm from the center of the shocked line, as shown in Fig. 2. At each position, the corresponding X-ray diffraction profile is recorded. For face-centered-cubic (FCC) metals, the diffraction structure factor for (1 1 0) and (0 0 1) are both zero and the reflections are absent (Cullity, 1978). So the (0 0 2) and (2 2 0) reflections are chosen for (0 0 1) and (1 1 0) orientation, respectively. For more details of X-ray micro-diffraction measurement, please refer to Chen et al. (2004).

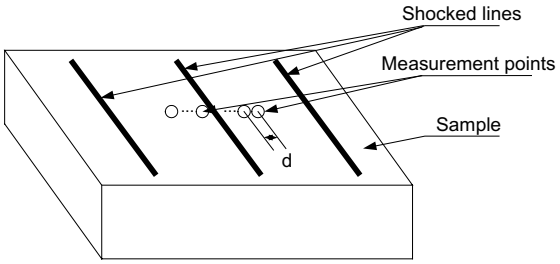

Fig. 2. X-ray micro-diffraction measurement arrangement (measurement points are along a line perpendicular to a shocked line, measurements were carried out within $\pm 100\,\mu m$ from the center of a shocked line, $d = 5\,\mu m$, within $20\,\mu m$ from the shocked line center, $d = 10\,\mu m$, elsewhere).

In addition to X-ray micro-diffraction, electron backscatter diffraction (EBSD), a diffraction technique for obtaining crystallographic orientation with sub-micron spatial resolution was applied to the shock peened samples, which allows quantitative study of crystalline texture as well. EBSD has some special advantages in micro-structure analysis over TEM. The sample preparation of EBSD is not destructive thus the nearly original state of the sample can be observed which is crucial to the shock peening study. A much larger area than TEM can be quantitatively and statistically analyzed. EBSD data was collected using a system supplied by HKL Technology (HKL Technology, 2001) and attached to a JEOL JSM 5600LV scanning electron microscope. The samples were briefly electrically polished to remove the mechanical scratches on the surface. The shocked region was accurately located using SEM before the EBSD measurements. All data were acquired in the automatic mode, using external beam scanning and employing a $1\,\mu m$ step size. The scan area is $100\,\mu m \times 150\,\mu m$ on the shocked surface and covered the shocked line center. Details about EBSD measurement can be found in Chen et al. (2004).

4. Principles of FFT evaluation

4.1. X-ray line profile analysis with Warren and Averbach method

With modern experimental techniques, it is possible to measure a X-ray line profile with sufficient accuracy to infer strain/stress distributions. The classic method is the Warren and Averbach method (Warren and Averbach, 1950), which is based on the Fourier analysis of the diffraction profiles and allows one to obtain distribution functions of the strains directly from the Fourier series coefficients. The key principles are briefly outlined below.

Consider a single crystal sample in which there is plastic deformation induced by laser shock peening. There is spacing change between the diffraction planes and an average strain over relatively large distances in the diffraction planes, causing a shift in X-ray line profile. The shock peening also produces dislocation arrays (Chen et al., 2004; Murr, 1981), such as small angle boundaries which subdivide the original single crystal into small coherent domains as grains in polygrained metal. As a result, the peened region can be regarded as polygrained metal (Warren, 1969). Those small mosaic like structures will cause the broadening of line profile since there are not as many planes to cause destructive interference away from the exact Bragg angle (Cullity, 1978). In fact both kinds of effects are superimposed in plastically deformed metals, and the X-ray line profile is both shifted and broadened.

From the analysis of Warren and Averbach (1950), the sample can be represented as columns of unit cells along the direction which is perpendicular to the diffraction plane in the reciprocal lattice space. The X-ray line profile can be considered as the combination of reflected X-ray from all pairs of unit cells.

In the reciprocal lattice space, the Bragg angle θ can be represented by the reciprocal of the spacing of two diffraction planes.

$$h = \frac{2\sin\theta}{\lambda \mid \mathbf{b} \mid} = \frac{2 \mid \mathbf{a} \mid \sin\theta}{\lambda}, \tag{1}$$

where **b** and **a** are the unit vectors from the origin to the diffracting points in reciprocal space and real space, respectively. h is the reciprocal of the lattice spacing, λ is the X-ray wavelength. Since the diffraction profile is the combination of the scattering of X-ray by periodically arranged atoms in the crystal lattice and can be considered as a periodic function in reciprocal lattice space. By converting the Bragg angle θ into h by Eq. (1), the measured X-ray line profile can be represented as the Fourier series in the reciprocal lattice space (Warren and Averbach, 1950)

$$P(2\theta) = \frac{KNF^2}{\sin^2\theta} \sum_{n=-\infty}^{+\infty} (A_n \cos 2\pi nh + B_n \sin 2\pi nh), \tag{2}$$

where $P(2\theta)$ represents the measured X-ray line profile vs 2θ, F is the structure factor and K is the angular factor. N represents the number of unit cells in the sample. The harmonic number n is related to L_n by $L_n = n/|\mathbf{b}|$, where L_n is the distance between a pair of unit cells in a column perpendicular to the diffraction planes. The real part of the Fourier coefficients is

$$A_n = \frac{N_n}{N_c} \cos 2\pi l Z_n, \tag{3}$$

where N_n is the number of cells in the entire sample having an nth neighbor in the same column, N_c is the average number of cells per column, and $l = h/|\mathbf{b}|$ is the number of unit cells between diffraction planes. Z_n is the distance between pairs of unit cells having an nth neighbor in the same column and can be represented as $Z_n = n\langle\varepsilon\rangle$, where $\langle\varepsilon\rangle$ is the average strain caused by crystal lattice distortion along the **a** direction. According to the analysis in Warren (1969), N_n/N_c depends only on the column lengths, so it is a size effect represented by A_n^{S}. The strain effect $\cos 2\pi l Z_n$ depends on the distortion in the crystal lattice represented by A_n^{D}. As mentioned before, the X-ray line profile after deformation is shifted and broadened. The A_n^{D} represents the spacing change between the diffraction planes and contributes to the line profile shift. The A_n^{S} represents a measure of the grain size and contributes to the profile broadening.

From the analysis above, the real part of Fourier coefficient A_n in Eq. (3) is the product of the size effect and the strain effect:

$$A_n = A_n^{\mathrm{S}} A_n^{\mathrm{D}}. \tag{4}$$

For small values of l and n, the product lZ_n is small and the term $\cos 2\pi l Z_n$ can be expanded to $1 - 2\pi^2 l^2 Z_n^2$ and the logarithm can be written

$$\ln(\cos 2\pi l Z_n) \approx \ln(1 - 2\pi^2 l^2 Z_n^2) \approx -2\pi^2 l^2 Z_n^2. \tag{5}$$

Since $Z_n = n\langle\varepsilon\rangle$, the measured Fourier coefficient is given by:

$$\ln A_n = \ln A_n^{\mathrm{S}} - 2\pi^2 l^2 n^2 \langle\varepsilon^2\rangle. \tag{6}$$

So Eq. (6) represents a straight line for $\ln A_n$ vs n^2 and its slope and intersection with $n = 0$ can be used to evaluate the strain and size effects.

4.2. Dislocation density evaluation using modified W–A analysis

From the analysis above, the size effect and strain effect can be obtained from Fourier analysis of X-ray profiles. According to the analysis of Chen et al. (2004) and Murr (1981), dislocation cell structures can be

formed after laser shock peening on single crystal Al and Cu sample and the residual strain/stress caused by those cell structure can be evaluated. However, in order to achieve further understanding of the microstructure induced by the laser shock peening, the dislocation density needs to be evaluated. According the work of Ungar and Borbely (1996), the analysis of Fourier coefficients of X-ray profiles shows that taking into account the dislocation effect on the profiles gives a modified method, known as the modified W–A analysis. This procedure enables a straightforward determination of dislocation density from X-ray line profile analysis.

In Ungar's model, for crystals containing dislocations, the diffraction profile is also considered as the combination of the diffracted X-ray for all unit cells in crystal as that in W–A method. However, the displacement of each unit cell is represented by the dislocation Burgers vector to account for the effect of dislocation structure and the real part of the Fourier coefficients of the X-ray line profile can be written as (Ungar and Borbely, 1996)

$$\ln A_n = c_0 - \rho^* n^2 \ln(R_e/n) + Q^* n^4 \ln(R_2/n) \ln(R_3/n), \tag{7}$$

where ρ^* is the "formal" dislocation density, directly available from a broadened profile without taking into account the effect caused by different types of dislocations. Q^* is given as the variation of the dislocation density, n is the harmonic number, and R_e is the outer cutoff radius of dislocations, which indicates the distribution range of dislocation stored energy. R_2 and R_3 are auxiliary constants. The true value of dislocation density is

$$\rho = \frac{2\rho^*}{\pi g^2 b^2 \overline{C}}, \tag{8}$$

where $\overline{C}$ is the average contrast factor for different type of dislocations (edge and screw) in the case of a particular *hkl* reflection and can be found in Ungar and Borbely (1996), b is the Burgers vector of dislocations which is $a/2\langle 1\,1\,0\rangle$ here for FCC metals and g is the diffraction vector. Thus, after calculating the real part of the Fourier coefficients A_n, the $\ln A_n$–n data can be fitted as non-linear curve using formula in Eq. (7). The parameters such as ρ^* can be determined in curve fitting using least-squares evaluation method and the dislocation density ρ can be evaluated by Eq. (8).

5. FFT evaluation results

5.1. Stoke correction using FFT

5.1.1. Stoke's correction for instrumental broadening

To correct for the instrumental broadening in the diffraction pattern of a sample, it is convenient to run a standard peak using a sample in which the mosaic size is large enough to eliminate all mosaic-size broadening. Three curves which are involved in the correction for instrumental broadening. $f(y)$ is the desired curve which would be obtained if there were no instrumental broadening. $g(z)$ is the curve representing instrumental broadening which is obtained from the standard. $h(x)$ is the curve from the sample, containing both the desired broadening and the instrumental broadening.

Since the profile from the sample is a convolution of the functions representing mosaic-size broadening and instrumental broadening. The Fourier coefficient of the $f(y)$-curve is then given by the simple relation:

$$F(n) = H(n)/G(n). \tag{9}$$

As mentioned before, multiple measurement points are chosen along a line perpendicular to a shocked line. The spacing between adjacent measurement points is maximum of 10 μm (when ±100 μm away from the center of the shocked line) and reduces to 5 μm within ±20 μm from the center of the shocked line, as shown

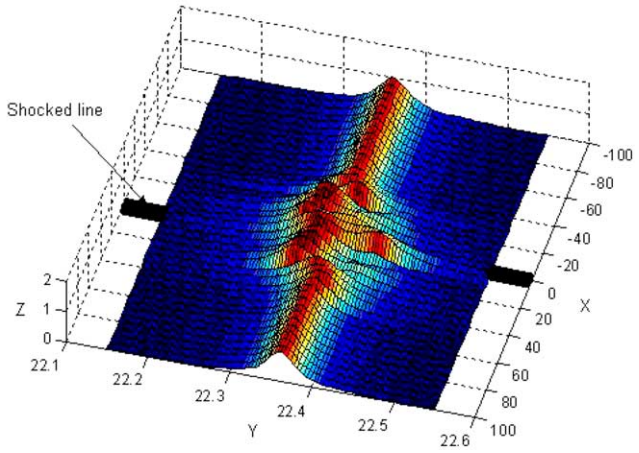

Fig. 3. 3D X-ray profile spatial distribution across the shocked line for (002) reflection of Al(001) sample (X-axis: distance from the shocked line center (μm); Y-axis: Bragg angle (Degree); and Z-axis: normalized diffraction intensity).

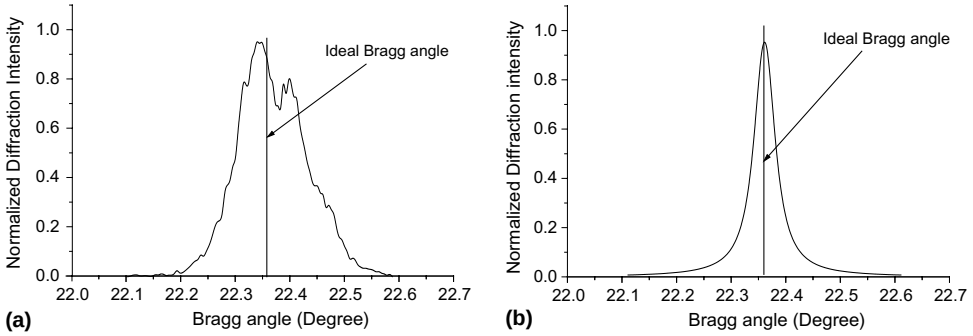

Fig. 4. Two cross sections of Fig. 3. (a) Profile measured at position at the center of shocked line, and (b) profile measured at unshocked position (100 μm away from the shock line center).

in Fig. 2. Fig. 3 shows the three dimensional spatial distribution of those measured X-ray profiles for Al(002) reflection. The X-ray profiles at shock peened center and unshocked region is shown in Fig. 4(a) and (b). It is clear that after shock peening, the X-ray profile was significantly broadened and became asymmetric compared to unshocked region. After using Stoke's correction, the profile broadening caused by the instrument can be eliminated and the effect due to laser shock peening can be evaluated. Here a typical $h(x)$ is the profile measured at the shocked region as in Fig. 4(a), containing both the desired broadening and the instrumental broadening. The curve $g(z)$ representing instrumental broadening in Fig. 4(b) is the profile measured at shocked free region which can be considered as prefect single crystal. Thus, the corrected X-ray profile $f(y)$ is obtained from Eq. (9).

5.2. Strain deviation estimate and comparison with FEM simulation

From the theory of Warren and Averbach (1950), for small values of l and n, the logarithm of the measured Fourier coefficient is given by Eq. (6). In order to understand better about shock-induced plastic deformation, it is necessary to study the corresponding inhomogeneous strain deviation in the depth

direction. For Al(002) reflection, $l = 2$, so the strain effect term can be represented as $-2\pi^2 l^2 n^2 \langle \varepsilon_l^2 \rangle$, in which $\langle \varepsilon_l^2 \rangle^{1/2}$ represented the value above or below the mean strain $\langle \varepsilon_l \rangle$ which represents the net strains over large distances. So the $\langle \varepsilon_l^2 \rangle^{1/2}$ can be considered as the inhomogeneous deviation from the mean strain caused by the laser shock peening in the [002] direction, which is in the depth direction perpendicular to the surface for Al(001) sample. If we choose n^2 as the X-axis and $\ln A_n(l)$ as the Y-axis, Eq. (6) represents a straight line with slope $K = -2\pi^2 l^2 \langle \varepsilon^2 \rangle$. Thus, the slope of this fitted line can be used to calculate the deviation from the mean strain from that X-ray profile as:

$$\langle \varepsilon_l^2 \rangle^{1/2} = \sqrt{\frac{K}{-2\pi^2 l^2}}. \tag{10}$$

The value of the deviation from the mean strain $\langle \varepsilon_l^2 \rangle^{1/2}$ indicates the extent of the inhomogeneous strain distribution and causes the broadening of X-ray line profile. For example, at the center of the shocked region (0 μm), the slope of fitted line is $K = -0.09035$, $l = 2$ for Al (002) reflection (Fig. 5(a)), so the

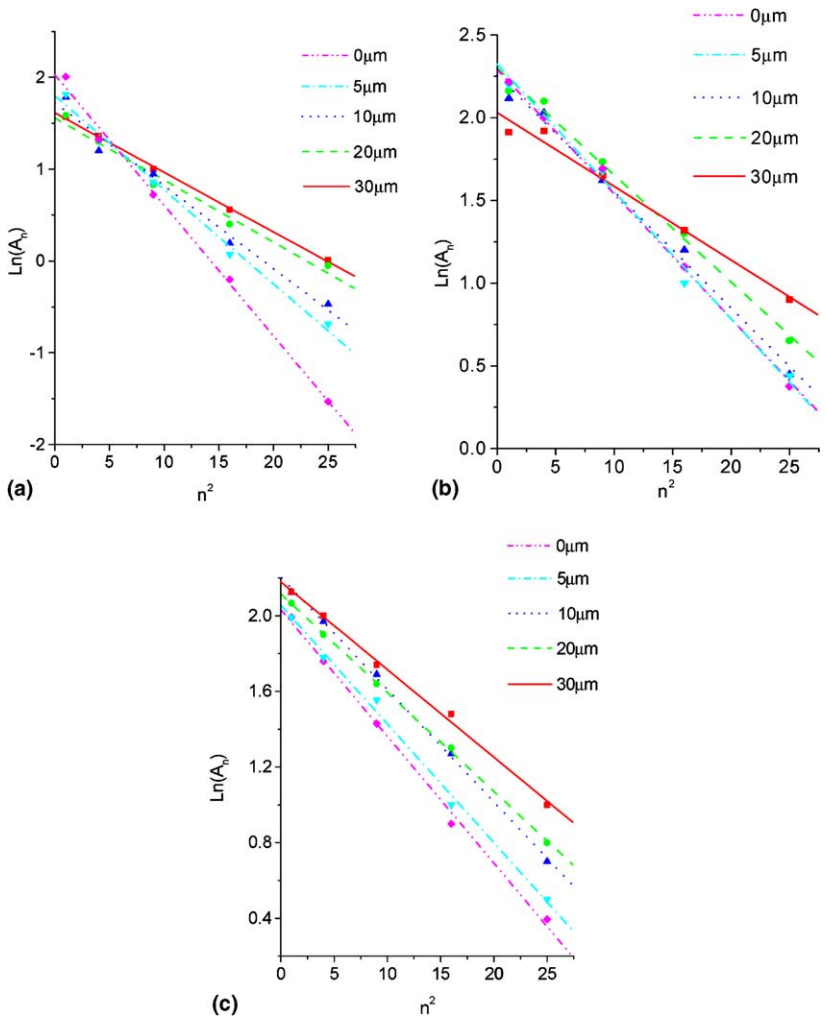

Fig. 5. Ln(A_n) vs n^2 lines at different position from the center of shocked line (A_n: the real part of corrected Fourier coefficient; and n: Fourier series number). (a) Al(002), (b) Al(220) and (c) Cu(220).

deviation from the mean strain $\langle \varepsilon_l^2 \rangle^{1/2}$ is 0.034 based on Eq. (10). In order to obtain the spatial distribution of the strain deviation, X-ray profiles at each position across the shocked line (from 30 μm left of the shocked line to 30 μm right) were processed using Fourier transformation with Stoke's correction mentioned before. Fourier number n^2 vs the natural logarithm of the real part of the corresponding Fourier coefficient $\ln A_n$ for different samples and reflections were shown in Fig. 5(a)–(c). It is clear that the magnitude of line slope increases from the position far away from the shock line center (30 μm) to the center of shock line (0 μm). So it shows the strain deviation increases gradually when the position move closer to the shocked center.

Fig. 6 shows the spatial distribution of calculated strain deviation from slope analysis for Al(0 0 1), Al(1 1 0) and Cu(1 1 0) sample shown in Fig. 5. The X-ray penetration depth is about 60 μm in the specimen. For all samples, the maximum strain deviation in depth direction occurs in the shocked line center and decreases with the position away from the center. The region of significant strain deviation is around ±40 μm from the center and the magnitude is maximum at the center to near zero when moving away from the center which indicates the extent of inhomogeneous strain distribution is largest at the shock line center. Also the strain deviation magnitude of Al(1 1 0) is significantly larger than that of Cu(1 1 0) probably due to strength difference. However, it is almost identical to that of Al(0 0 1) sample and indicates a weak dependence of strain variation with crystalline orientation under the conditions used.

The nonuniform strain deviation is caused by the dislocation structure induced by the plastic deformation in μLSP and contributes to the hardness increase in the shocked region, which is the main effect of shock peening. The trend of strain deviation was compared with FEM simulation qualitatively for all samples and Fig. 7 shows a typical strain distribution under laser shock peening for Al(0 0 1) sample. It is clear that the strain caused by shock peening is compressive and is concentrate in the region about ±25 μm from the shocked line center, which indicates that this region has the greatest potential for strain deviation, in good agreement with the result from Fourier analysis of X-ray profile.

5.3. Mosaic size estimate and comparison with EBSD

Mosaic size broadening is represented by a cosine Fourier series similar to that developed for distortion broadening and hence the Fourier coefficients A_n give very general method of handling either effect. From the analysis of Warren and Averbach (1950), the initial slope of the A_n vs n curve is

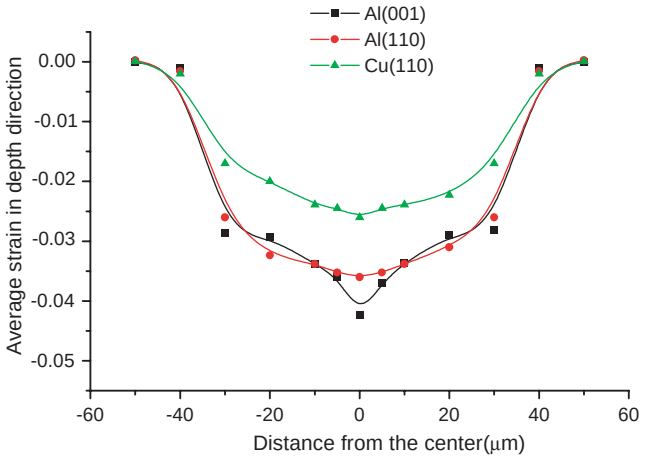

Fig. 6. Spatial distribution of strain deviation in depth direction evaluated from slope analysis shown in Fig. 5.

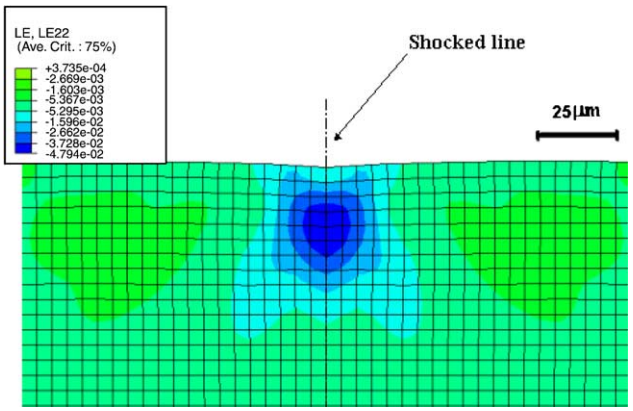

Fig. 7. Typical FEM simulation result of strain distribution in depth direction, A1(001) sample: $200 \times 80\,\mu m$ as shown, total simulation region is $800 \times 400\,\mu m$, deformation factor = 5 for viewing clarity.

$$\left(\frac{dA_n}{dn}\right)_{(n=0)} = -\frac{1}{\overline{N}_3}, \tag{11}$$

where $\overline{N}_3 a_3$ is the average column length and hence an average mosaic size in the direction a_3.

Also we have

$$1/2 = (2a_3/\lambda)(\sin\theta - \sin\theta_0), \tag{12}$$

where λ is the wavelength of X-ray, θ is the maximum angle in X-ray profile and θ_0 is the ideal Bragg angle. So if the measurement of mosaic size broadening are expressed in terms of a plot of the Fourier coefficients A_n vs n, the initial slope of the curve gives directly the average column length, which is the effective mosaic size in that direction.

Consider the Fourier transformed Stoke's correction for the X-ray profile of (002) reflection for Al(001) sample at each position. Fig. 8(a) shows the curves of real part of corrected Fourier coefficient A_n vs n for

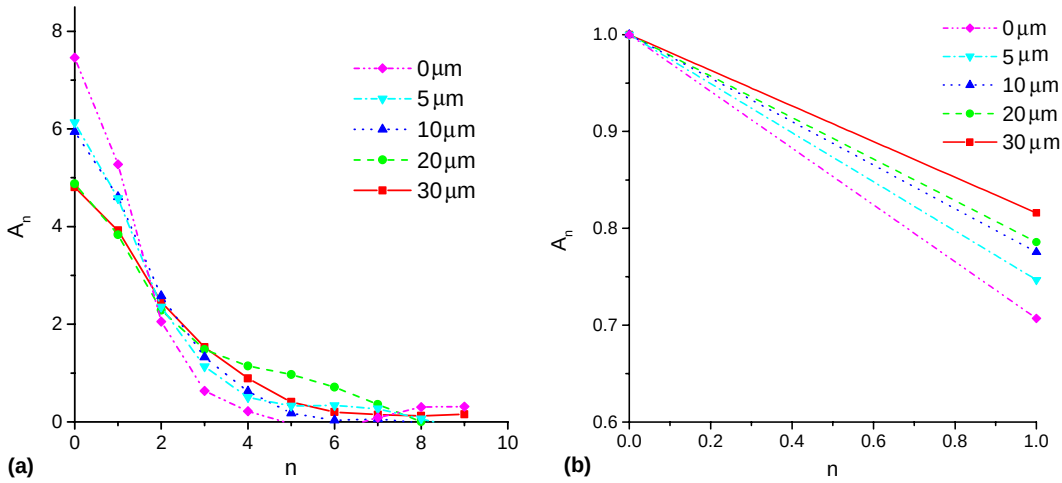

Fig. 8. (a) A_n vs n for different positions away from the shock line center for Al(001) sample (A_n: the real part of corrected Fourier coefficient; and n: Fourier series number). (b) The initial slope of A_n vs n curves for Al(001) sample.

different position away from the shock line center. Fig. 8(b) shows the initial slope of those curves (the line connecting the first two points in A_n–n curve) and A_n has been normalized here. If the intercept of these lines with the X-axis is D, and the initial slope of curve is K, then the average mosaic size D at that position can be evaluated as

$$D = \left(\frac{1}{K}\right) \cdot a_3. \tag{13}$$

For example, for position at the center of shock line (0 μm), $\lambda = 1.54062$ Å, $\theta = 22.596°$, $\theta_0 = 22.36°$, so $a_3 = 101.2$ nm and the initial slope K is 0.293, so the average mosaic size is 345.3 nm. Using the similar method, the average mosaic size at different positions can be calculated and the spatial distribution can be obtained for all samples.

Fig. 9 shows the spatial distribution of average mosaic size for Al(0 0 1), Al(1 1 0) and Cu(1 1 0) sample evaluated from the X-ray profile analysis mention above. It can be seen that the average mosaic size decreases near the shock line center for all samples. In the region of ±20 μm from the center, the mosaic size is around 1 μm to 0.7 μm and increases sharply to over 100 μm beyond this range. This is reasonable since the shock peening effect is higher in the shock line center and larger plastic deformation favors the formation of mosaic structure. It is interesting that the results of Al(0 0 1) and Al(1 1 0) are quite similar, for Cu(1 1 0) sample, the average mosaic size is larger than that of Al sample and the submicron mosaic size is limited in the ±10 μm region. The overall trend is consistent with the spatial distribution of strain deviation and the influence of different crystalline orientation is less than different materials.

In addition to using X-ray profile analysis to obtain the mosaic size distribution after laser shock peening, EBSD measurements were made on all samples' surface and mosaic structure was analysis and compared with the result from X-ray. Mosaic structures can be quantitatively analyzed through EBSD measurements because EBSD is based on sub-micron spatial accuracy data acquisition of misorientation angles, and the misorientation angle accuracy is less than one degree. Fig. 10 shows the micro-structures of mosaic for Al(0 0 1) and Cu(1 1 0) sample. The thin black lines show mosaic boundaries whose misorientation angles are larger than 3°. The line I represents laser shocked line. The cross sections represented by lines 1, 2 and 3 with spacing 12.5 μm are made perpendicular to the shocked line. The spatial distribution of mosaic size along the three lines is shown in Fig. 11. It is observed that within the shock peening region

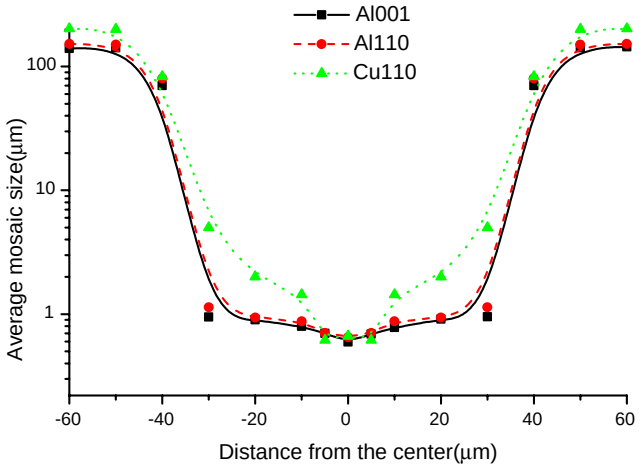

Fig. 9. Spatial distribution of average mosaic size from initial slope analysis (Fig. 9).

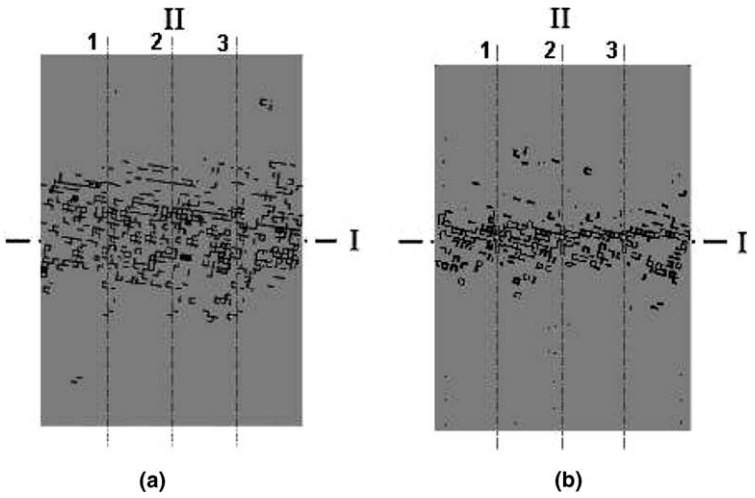

Fig. 10. Mosaic micro-structure distribution on shocked peened surface measured with EBSD (50 μm × 80 μm). Three cross sections perpendicular to the shocked line are indicated by 1, 2 and 3; (a) Al(1 1 0) sample, (b) Cu(1 1 0) sample.

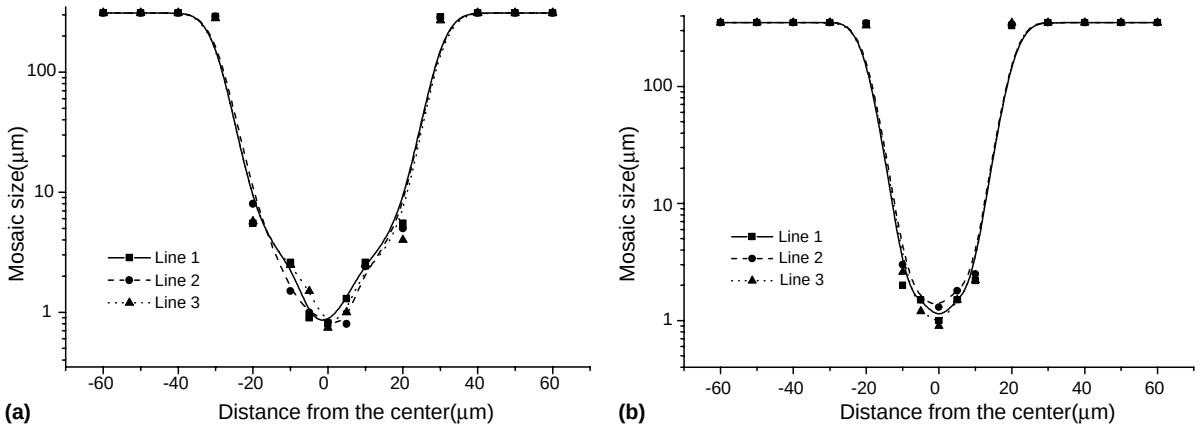

Fig. 11. Spatial distribution of mosaic size along the three cross sections perpendicular to the shocked line. (a) Al(1 1 0), (b) Cu(1 1 0).

(±20 μm from the shock line center for Al and ±10 μm for Cu), it has a larger increase in mosaic structure and the smallest mosaic size (0.8 μm for Al and 1 μm for Cu) is dominant in the center and become larger away from the shock peened region. This is consistent with the result obtained from the X-ray profile analysis mentioned before.

The substantial increase of sub-structures is related to the strength and hardness improvement in LSP. The formation of mosaic structures has an effect similar to grain refinement. According to Murr (1981), the yield strengths of Copper and nickel increase after LSP. As a result of a mosaic size refinement, the shocked area is strengthened according to well-known empirical relationship such as the Hall–Petch relation between average grain size and the yielding limit of a bulk metal since metal in shocked area can be considered as polycrystalline metal due to the mosaic structure:

$$\sigma_Y = \sigma_0 + \frac{k}{\sqrt{d}}, \tag{14}$$

where σ_Y is the flow stress, σ_0 and k are material dependent constants, and d is the average mosaic size. As a result, the hardness and yield strength of material are expected to increase after μLSP.

As mentioned before, the nonuniform strain deviation caused by the dislocation structure in μLSP also contributes to the hardness increase in the shocked region. Thus, both strain deviation and mosaic size refinement contribute to the hardness and strength increase after μLSP. However, the quantitative relation between strain deviation and hardness is still missing. In order to investigate which mechanism is dominant, nanoindentation needs to be applied to measure the hardness change across the shocked line. If the surface hardening is mainly caused by the mosaic size refinement, the hardness increase can be estimated using Eq. (14) and should be close to the result from nanoindentation measurement. Otherwise, the difference of hardness may correspond to the nonuniform strain deviation in the shock peened region.

5.4. Dislocation density estimate using modified W–A model

The recorded X-ray profiles for the single crystal Al and Cu samples (Chen et al., 2004) strongly suggest the existence of dislocation cell structure. In fact, dislocation cell structures were observed via transmission electron microscopy (TEM) in laser shock peened metals such as Copper (Stouffer and Dame, 1996). It accompanies the generation and storage of a higher dislocation density than that from quasi-static deformation processes.

It is of interest to study the magnitude and spatial distribution of dislocation density under μLSP. Within the formalisms of the kinematical scattering of X-rays and the linear elasticity theory of dislocations, the modified Warren–Averbach method was used to evaluate dislocation density via X-ray profile analysis (Ungar and Borbely, 1996). According to Eq. (7), non-linear least-squares curve fitting was applied to the plot of the Fourier coefficients $\ln(A_n)$ vs n in Fig. 12. All six parameters c_0, ρ^*, Q^*, R_e, R_2, and R_3 were calculated through six curve fitting parameters $P1$ to $P6$ using standard methods. After obtaining the formal dislocation density ρ^*, the true values of dislocation density was calculated by Eq. (8).

Fig. 12 shows the curve fitting results for the real part of corrected Fourier coefficient $\ln A_n$ vs n at different positions from Al(0 0 2) reflection profile. It is clear to see that for positions closer to the shock line center, the curve slopes down more significantly than further away, which indicates the extent of the laser shock peening. Using the same method, X-ray profiles of Al(1 1 0) and Cu(1 1 0) were analyzed and the

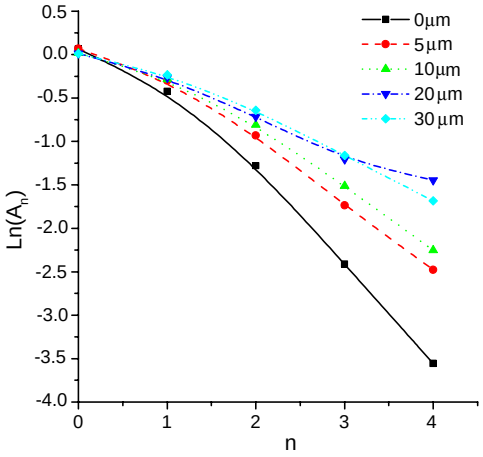

Fig. 12. Typical curve fitting result for Ln(A_n) vs n for Al(0 0 1) sample (A_n: the real part of corrected Fourier coefficient; and n: Fourier series number).

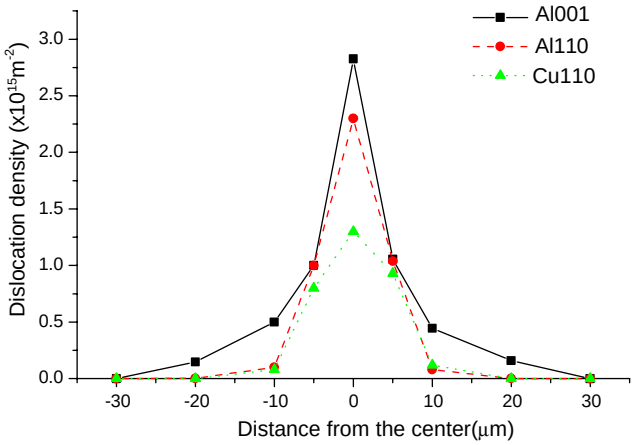

Fig. 13. Spatial distribution of dislocation density obtained from curve fitting analysis shown in Fig. 12.

dislocation density spatial distributions were evaluated. Fig. 13 compares the dislocation density distribution for Al(0 0 1), Al(1 1 0) and Cu(1 1 0) samples, where it is evident that the highest density occurs at the shock line center and decays slowly to the outer edge. It can be seen that the dislocation structure is most significant in Al(0 0 1) sample and less in Al(1 1 0) sample, and the least for Cu(1 1 0) sample.

This can be explained by noting that the most apparent feature controlling micro-structures or microstructure development in FCC metals and alloys is the stacking-fault free energy. From the analysis of Chen et al. (2004), easy cross slip is an essential mechanism for dislocation formation. In high stacking-fault free energy materials, the stacking fault energy limits the partial dislocations and promotes cross slip of dislocations from one plane to another. Therefore high stacking-fault free energies favor the formation of dislocations by cross slip mechanism. Typically, dislocation structures are formed in shock-loaded metals when the stacking-fault free energy is greater than about 60 mJ/m^2 (Stouffer and Dame, 1996). For stacking-fault free energy below about 40 mJ/m^2, planar arrays of dislocations stacking faults, and other planar micro-structures result. Al is the FCC metal with the highest stacking-fault free energy (168 mJ/m^2) and Copper is 78 mJ/m^2 (Murr, 1981). As a result, the dislocation cell structure can be generated easier in Aluminum than in Copper.

It is well known that in FCC metals the plastic slip systems are the $\{1\,1\,1\}$ family of planes in the $\langle 1\,1\,0\rangle$ family of directions, for a total of 12 possible slip systems. From the analysis of Chen et al. (2004) and Stouffer and Dame (1996), cross slip occurs with greater difficulty in the (1 1 0) orientation, since there is no common slip direction between different slip planes. However, in (0 0 1) orientation, cross slip can be generated between the $(1\,1\,1)$ $\langle 1\,0\,\bar{1}\rangle$ and $(\bar{1}\,1\,\bar{1})\langle 1\,0\,\bar{1}\rangle$ slip systems. Thus, the cross slip occurs much easier in (0 0 1) shock peened orientation than in (1 1 0) orientation and this favors the formation of dislocation structures in (0 0 1) orientation.

6. Conclusions

X-ray micro-diffraction profile analysis using Fourier transformation was realized for single crystal Al and Copper sample subjected to micro-scale laser shock peening. The asymmetric and broadened diffraction profiles registered at each location were analyzed by classic Warren and Averbach method (Warren and Averbach, 1950) and modified W–A method proposed by Ungar and Borbely (1996). Spatial distribution of strain deviation, mosaic size and dislocation density were estimated. FEM simulation and EBSD

were applied to all samples to verify the result. Micron level spatial resolution (down to 5 μm) was achieved. The nonuniform strain is existed within ±30 μm from the shocked line center, after which the strain is much more uniform. The result was found consistent with FEM simulations. In addition, the results were seen to depend more on the material than the crystal orientation. Sub-micron mosaic-like substructures were formed in the region ±20 μm from the shocked line center as determined both from diffraction profile analysis as well as EBSD. The asymmetric and broadened profiles are strongly indicative of dislocation formation during LSP and material in (0 0 1) orientation and material with higher stack fault energy (Al) shows higher dislocation density under laser shock peening.

Acknowledgement

This work is supported by the National Science Foundation under grant DMI-02-00334. Dr. Jean Jordan-Sweet of IBM Watson Research Center provided assistance in using the X-ray micro-diffraction apparatus at the National Synchrotron Light Source at Brookhaven National Laboratory. Assistance in technical details in sample preparation for EBSD and data analysis by Dr. Yongxue Gang, and Mr. J.B. Chou is also appreciated. JWK gratefully acknowledges support with NSF grant CMS-0134226. This work also used the shared experimental facilities that are supported primarily by the MRSEC Program of the National Science Foundation under Award Number DMR-0213574 and by the New York State Office of Science, Technology and Academic Research (NYSTAR).

References

ABAQUS/Standard User's Manual, 2002. Version 6.2, Hibbit, Karlsson and Sorensen, Inc., Pawtucket, RI, USA.

Asaro, R.J., 1983. Micromechanics of crystals and polycrystals. Advances in Applied Mechanics 23, 1–115.

Chen, H.Q., Yao, Y.L., Kysar, J.W., 2004. Spatially resolved characterization of residual stress induced by micro scale laser shock peening. ASME Journal of Manufacturing Science and Engineering 126 (2), 226–236.

Chen, H.Q., Kysar, J.W., Yao, Y.L., 2004. Characterization of plastic deformation induced by micro scale laser shock peening. ASME Journal of Applied Mechanics. 71 (5), 713–723.

Cullity, B.D., 1978. Elements of X-ray Diffraction, second ed. Addison-Wesley Publishing Company Inc., London, pp. 268–270.

HKL Channel 5^{TM} User's Manuel, 2001, HKL Technology, Danbury, CT.

Huang, Y., 1991. A user-material subroutine incorporating single crystal plasticity in the ABAQUS finite element program, Mech Report 178, Division of Applied Sciences, Harvard University, Cambridge, MA.

Krivoglaz, M.A., Ryaboshapka, K.P., 1963. Theory of scattering of X-rays and thermal neutrons by real crystals. Fizika Metallov I Metallovedenie 15, 18–25.

Kysar, J.W., 1997. Addendum to "A user-material subroutine incorporating single crystal plasticity in the ABAQUS Finite element program, Mech Report 178", Division of Engineering and Applied Sciences, Harvard University, Cambridge, MA.

Murr, L.E., 1981. Microstructure-mechanical property relations. In: Shock-wave and High-Strain-Rate Phenomena in Metals. Plenum Press Inc., New York, pp. 607–671.

Stouffer, D.C., Dame, L.T., 1996. Inelastic Deformation of Metals. John Wiley & Sons, Inc., New York, pp. 12–15.

Ungar, T., Borbely, A., 1996. The effect of dislocation contrast on X-ray line broadening: A new approach to line profile analysis. Applied Physics Letter 69, 3173–3175.

Warren, B.E., Averbach, B.L., 1950. The effect of cold-work distortion on X-ray patterns. Journal of Applied Physics 21, 595–599.

Warren, B.E., 1969. X-ray Diffraction. Addison-Wesley, Reading, MA (Chapter 13).

Wilson, A.J.C., 1942. Imperfections in the structures of cobalt. II. Mathematical treatment of proposed structure. Proceedings of Royal Society of London Series A 180, 277–285.

Zhang, W., Yao, Y.L., 2000. Micro scale laser shock processing of metallic components. ASME Journal of Manufacturing Science and Engineering 124 (2), 369–378.

Zhang, W., Yao, Y.L., 2001. Feasibility study of inducing desirable residual stress distribution in laser micromachining. Transactions of the North American Manufacturing Research Institution of SME (NAMRC XXIX) 2001, 413–420.